

# **Geometric Correction of SEM Images**

---

Jay P. Kapur

Masters Project Report

Dr. David Casasent

Graduate Advisor

---

## Table of Contents

|  |    |
|--|----|
| Table of Contents .....                          | 1  |
| Abstract.....                                    | 2  |
| Introduction.....                                | 3  |
| Why do we need accurate SEM images?.....         | 3  |
| Sources of Distortion in SEM Images .....        | 4  |
| Correcting Geometric Distortions .....           | 8  |
| Background .....                                 | 8  |
| Correction Using A Piecewise Approach.....       | 10 |
| Affine Transforms for Piecewise Correction ..... | 12 |
| The Correction Algorithm.....                    | 16 |
| Bibliography.....                                | 23 |

## Abstract

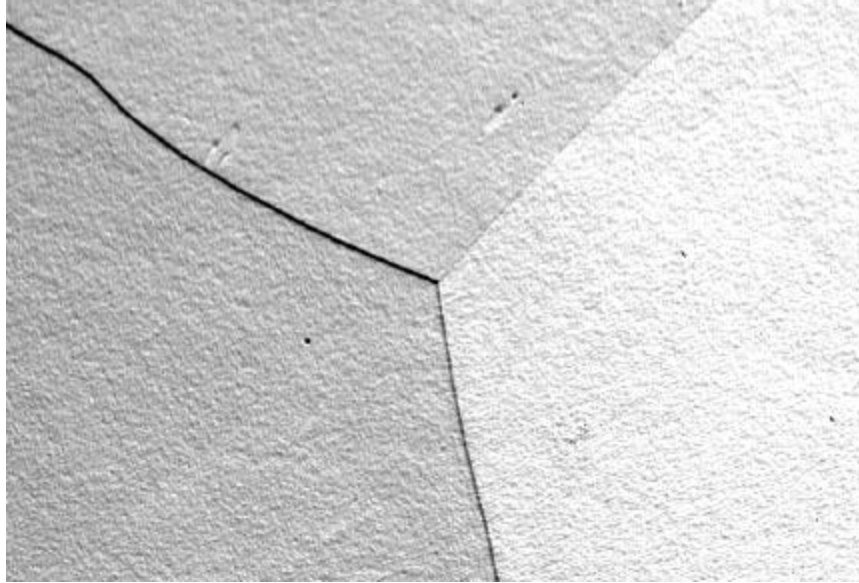
While the resolution that can be achieved with scanning electron microscopy is unquestioned, the accuracy of any scientific measurements derived from scanning electron microscopes (SEM) are limited due to a variety of sources of distortion in the microscope and the equipment setup. For this reason, SEM images are not often used for making geometric measurements. To facilitate such measurements, a consistent and accurate means of correcting geometric distortions using a piecewise affine transform is described and implemented. This method works independently of specific microscope settings and therefore generalizes well to compensate for nearly any source of geometric distortion in images. The result is a technique that can be applied with no knowledge of the distorting functions. The distortion correction routine is performed once on an image of a calibration standard, and the associated lookup table is used to correct all subsequent images. Collection of large amounts of high quality data from scanning electron microscope imagery, even when many images are required to capture an entire sample, is now possible with automated correction and registration of adjacent images.

## Introduction

Why do we need accurate SEM images?

Often scanning electron microscopy is used to observe incredibly small objects not visible to the naked eye for the purposes of qualitative (not quantitative) study. SEM has benefited researchers from the biologist studying bacteria to the engineer designing integrated circuits. The majority of these applications do not require accurate representation of lines, angles, and curves in the images. Typically the only quantitative analysis in any of these observations is the level of magnification, so that one is able to judge the relative size of the object being studied. However, accuracy in SEM images is becoming increasingly important in research environments, especially those relating to crystallography [1,12].

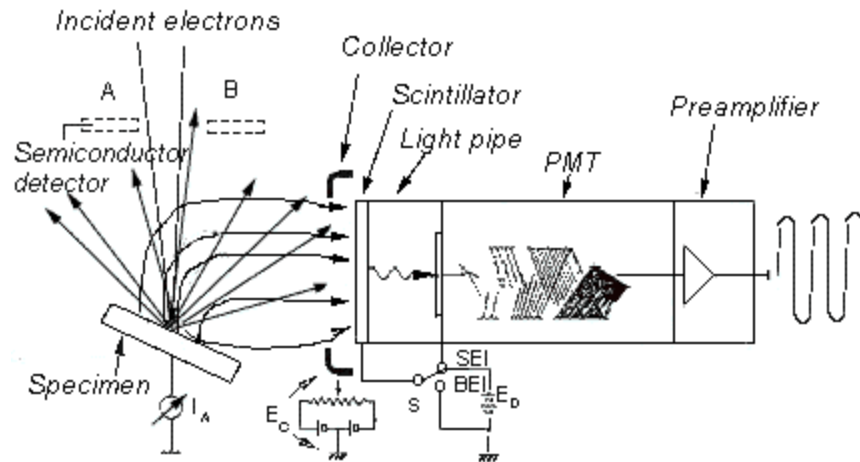
Of particular interest to researchers working on the Mesoscale Interface Mapping Project (MIMP) in the Department of Material Science Engineering at Carnegie Mellon University (CMU) are grain boundaries, the border between two or more crystalline structures in a material. Features such as the curvature of a boundary, the angles made at the triple junctions where three grains meet (Figure 1), and the orientations of grains are being studied to better understand how intergranular behavior relates to material stress and failure. These researchers depend on quantitative scientific observations of the microscopic polycrystalline structure to form or verify their hypotheses. Geometric correction is necessary to provide better quantitative measurements; the accuracy of angle measurements at triple junctions (dihedral angles) is of particular importance [12].



- Figure 1: Backscatter Electron Image of a triple junction in Aluminum

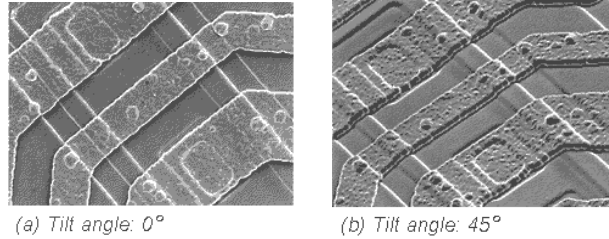
### Sources of Distortion in SEM Images

The sources of distortion in SEM images are numerous and vary in their affects and severity. Many of the distortions are not specifically geometric (*i.e.* added noise, blurring, low sharpness, or low contrast); we do not address them. The single greatest source of geometric distortion, our primary concern, is specimen tilt.



• Figure 2: Setup for secondary electron emission with specimen tilted [2]

Typically, measurements of specimen geometry are not performed when the microscope stage is tilted. However, tilting the specimen and using secondary electron emission (Figure 2) can provide benefits such as improved contrast and specimen topography information (Figure 3). Moreover, the MIMP researchers at CMU specifically require a tilted specimen because they perform electron back-scatter probes (EBSP) in each grain around each triple junction. A tilted sample is needed to provide high contrast EBSP images (the EBSP data provide grain orientation information). The secondary electron image (SEI) data is used to determine locations of triple junctions, and the EBSP data is taken in the grains around triple junctions. The specimen must be in the same (tilted) location while collecting the SEI and EBSP data. Thus, the sample must be tilted while taking the SEI images.

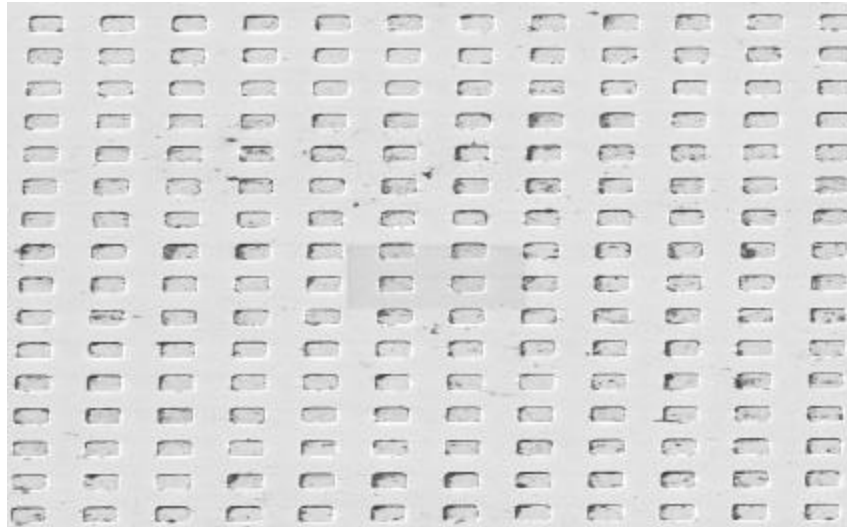


- Figure 3: Improvement of topographical information using secondary electron emission with specimen tilt

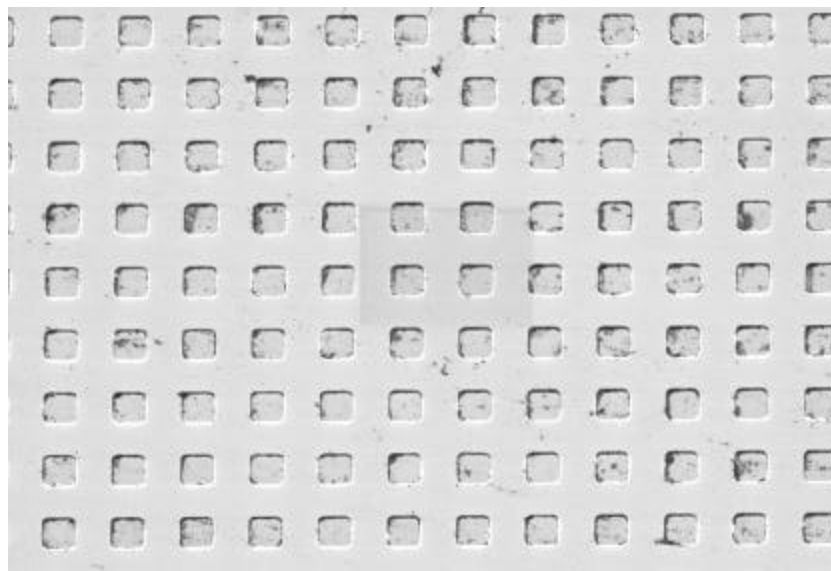
The distortion caused by specimen tilt, seen in Figure 4 for a specimen at 60°, is characterized by a demagnification of  $1/\cos\theta$  along the tilt axis (vertical in Figure 4) [2]. The SEM image in Figure 4 is of a calibration standard containing squares arranged in a regular pattern. Note that the uncorrected image in Figure 4 shows the squares with a much different height-to-width ratio due to the demagnification caused by specimen tilt. The distortion is not simply a demagnification, because the SEM images are perspective projections. Looking at the image in Figure 4, we can see that vertical lines do not appear at right angles to horizontal lines as they should; the vertical lines are slanted 3° to the right.

Modern scanning electron microscopes are often equipped with scan rotation and tilt (SRT) correction to compensate for demagnification caused by specimen tilt (Figure 5). Such systems are often deemed good enough for qualitative observations, but don't always provide the level of precise correction needed for quantitative geometric measurements. The SRT correction built into the Philips SEM used by the MIMP researchers gives the result shown in Figure 5. As seen, it only corrects the  $1/\cos\theta$  demagnification in the vertical direction. (Note that only a portion of the original distorted image appears in the SRT corrected result in Figure 5 due to a limitation on the image size when using the Philips SEM.) Careful inspection of the corrected image in Figure 5 shows the image is still skewed by 3° in the vertical direction. This is an artifact of the perspective projection, which the SRT correction does not account for. We could use a global projective transform to correct this distortion, but

there are other sources of distortion present in SEM images which this approach cannot address.



• Figure 4: SEM image with 60 degree sample tilt at 1000X



• Figure 5: Result of automatic tilt correction

The other sources of distortion include scan generator error, external magnetic fields, and user error [1,2]. Scan generator error can have deleterious effects on SEM image geometry. Scan generator error or distortion in the scanning frame results from non-linearities inherent



in the SEM hardware [3]. These distortions can be corrected with electronic hardware now commonly found in modern SEM devices. External magnetic fields, arising from any number of sources, can alter the electron beam and add non-linear geometric distortions to the image. Finally, user error can result in geometric distortion, such as in the case of improperly setting the angle of the sample with respect to the beam axis. The scan generator distortions can be corrected with internal hardware[3], but the other sources of distortion cannot. With the exception of sample tilt, none of these distortions can be predicted, they must be measured. We can address distortion caused by sample tilt, scan generator error, external magnetic fields, and user error with a single technique. This requires a flexible distortion correction method, such as the one we discuss in the following section.

## Correcting Geometric Distortions

### Background

The method we employ is a software based approach which is capable of addressing all geometric distortions as a post-imaging step on the PC. The method can complement any correction systems present internally in the SEM. Early SEM systems with analog outputs did not facilitate efficient correction and as a result high precision measurements were, and still are, generally not taken from SEM images. Hardware based correction systems have been integrated with microscopes to address specific problems, such as scan generator function correction [3]. With digital output from the SEM and a software based approach, more general correction is made possible.

Geometric correction can be thought of as a mapping from distorted image space to undistorted space. This mapping is represented as a function that transforms a source coordinate  $(u, v)$  in the distorted image to a destination coordinate  $(x, y)$  in the corrected image:

$$x = f(u,v) \quad y = g(u,v).$$

The transformation can just as easily be considered in the reverse direction, from a corrected space coordinate  $(x,y)$  to a distorted space coordinate  $(u,v)$  as:

$$u = p(x,y) \quad v = q(x,y).$$

The forward mapping will take every pixel in the distorted image and place it in the corrected image, but there is a possibility that the corrected image will have some "holes" because this method does not assure that every pixel in the corrected image will be used. When the mapping is done in the reverse direction, the corrected image is guaranteed to have every pixel mapped to a pixel in the original distorted image. Thus, in our system, we choose to use the reverse mapping so as to avoid holes in the corrected image.

Some research efforts have focused on designing specific correction functions for specific imaging devices. One example is a correction algorithm for endoscope imaging based on a specific model of the "barrel" distortion in medical endoscope images [4]. SRT correction for sample tilt distortion in SEM uses this approach to compensate for the demagnification. These methods attempt to predict the distorting function, this is a complex task and is not possible for external magnetic field or user setup distortions. Our approach is to correct a distorted image of a calibration standard, determine the distortion analytically (not theoretically), and then apply the transformation to all subsequent images using a lookup table which stores the pixel mappings. Another benefit is that this approach results in a generalized method that can be applied to other imaging systems besides SEM.

Many correction methods using this approach (correcting a known calibration pattern) have been used, which we now discuss. A common general correction method is global polynomial warping. This method fits an  $N$ -th order polynomial to specified points in a

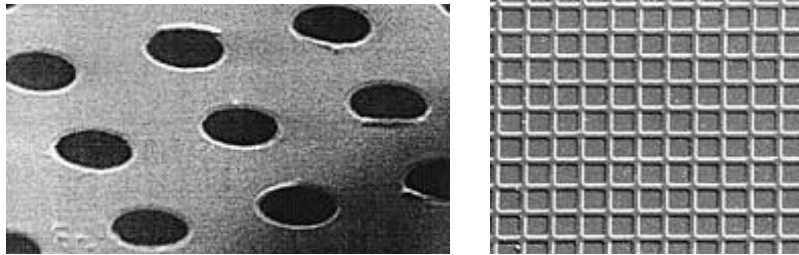
reference image in order to model the distortion. Polynomial warping has been applied to SEM [5] as well as numerous other imaging devices [6]. The approach is appealing because of its simplicity, but it is not guaranteed to produce the best result, since such a global approach attempts to fit a function to the entire image. This means that some regions of the image may not be corrected as well as others (or might even have increased distortions) and there is always the question of determining the best N-th order polynomial to use. We found that applying the global polynomial warp (with bilinear interpolation of pixels) to the MIMP data gave poor accuracy and made registration of adjacent sector images difficult.

### Correction Using A Piecewise Approach

Our approach is to use a general correction method based on a piecewise transform. A piecewise approach means that a reference distorted image (an image of a calibration standard with a regularly repeated pattern) is broken up into regions bounded by points (sometimes called tie-points or control points [7]) at vertices of primitive geometric shapes. The primitive shape is typically a triangle when using the affine transform or a quadrilateral when using a projective transform. The distortion for each local region is modeled by using the control points to determine the transform equation coefficients. The piecewise correction method allows a different correction to be applied to each local region. The piecewise transform is commonly used in computer graphics for image warping and has been applied to various applications, including X-ray image correction [8,11], but bilinear interpolation was used and methods to handle points on triangular boundaries were not addressed. The procedure can be easily automated and the transform method (affine, projective, curvilinear) can be chosen to suit the application.

The calibration standard is an object with a regular pattern placed on its surface for the purpose of observing image distortions. The image taken of the calibration standard is referred to as the reference distorted image. The reference distorted image is separated into

the desired regions by locating landmarks and using their coordinates as control points (points whose distances in the calibration standard and pixel coordinates in the reference distorted image are known). The only requirement of the calibration standard is that it contain features spaced at known real world distances and, for completely automated systems, that the features be easily detected by an image processing routine. For SEM images, we use a calibration standard such as the ones in Figure 6, where the landmarks are of known sizes and occur at known intervals as certified by the manufacturer or an independent standards organization. The landmarks can be the centers of circles (or squares), the crossing points of two lines, or any other repeating feature. If reduced computations are desired and if a high number of local transform regions are not necessary for good accuracy, the number of local transforms can be reduced by only using every N-th landmark as a control point. For SEM images, we have found that this latter approach produces acceptable results.

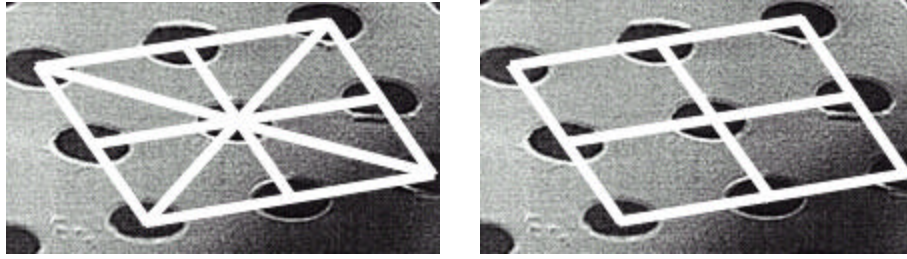


• Figure 6: SEM calibration standards

Because the positions of the control points occur at known distances, the mapping between the control points in the reference distorted image and the ideal corrected image are known. Furthermore, the pixel to real world distance conversion is also implicit. We generate an empty buffer to hold the corrected image and place the control points in their ideal locations in this corrected image buffer.

The control points are used to form the boundaries of the local regions. The case of nine control points arranged in a 3x3 pattern is considered in Figure 7, where the control points

are the centers of the circular landmarks. Sets of three control points form a triangle region and create eight total local regions as in Figure 7a. Using sets of four control points form quadrilaterals and creates four total local regions as in Figure 7b. Each set of control points which form the vertices of a region are used to solve for the coefficients of the chosen transform function. The transform function with the determined coefficients is then used to map all points within each local region. By storing the mapping for each local region in a single lookup table, future correction of images taken with the SEM can be performed quickly.



(a)

(b)

• Figure 7: Using 3x3 control points to form triangle regions (a) or square regions (b)

### Affine Transforms for Piecewise Correction

We choose to model the local distortion as an affine transform. The affine transform allows a combination of 2D scale, rotation, and translation for six degrees of freedom. Mathematically the transform is written as:

$$u = a + by + cx \quad v = d + ey + fx.$$

Or in matrix form as:

$$\begin{bmatrix} u \\ v \\ 1 \end{bmatrix} = \begin{bmatrix} a & b & c \\ d & e & f \\ 0 & 0 & 1 \end{bmatrix} \begin{bmatrix} x \\ y \\ 1 \end{bmatrix}$$

The affine transform coefficients  $(a,b,c,d,e,f)$  can be computed from three 2D points, thus the local regions used in the correction are triangles whose vertices are three control points as in Figure 7a. With an affine transform, any parallelogram can be warped to a square. Parallel lines are preserved with an affine transform.

Higher-order transforms can also be used to warp any quadrilateral into a square while still preserving straight lines (eight degree of freedom projective transform), or to fit curves between control points (curvilinear transforms), but this will not preserve straight lines. The projective transform is defined as:

$$u=(ax+by+c)/(gx+hy+i) \quad v=(dx+ey+f)/(gx+hy+i).$$

The projective transform, requiring four control points (assuming  $i=1$ ), can be implemented in such a manner that matrix inversion is not required [9], making it a viable alternative to the affine transform. The computational costs this method are much higher than when using affine transforms, but not prohibitive. Higher-order transforms, such as the curvilinear transforms are sometimes called rubber-sheeting transforms because their warps do not preserve straight lines. Examples of curvilinear transforms are

$$u=ax+by+cxy+d \quad v=ex+fy+gxy+h$$

or

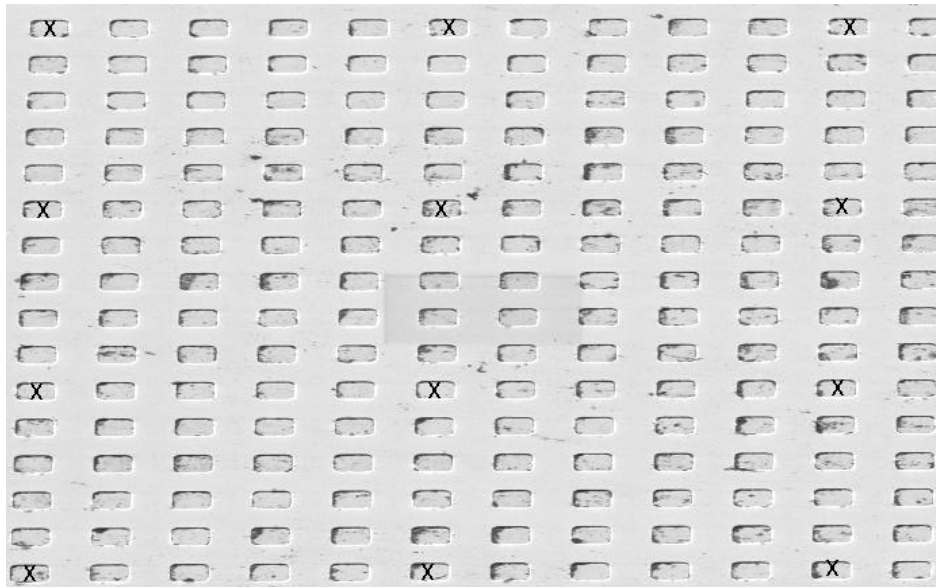
$$u=ax+by+cx^2+dy^2+exy+f \quad v=gx+hy+ix^2+jy^2+kxy+l.$$

The correction result with curvilinear transforms can be similar to the global polynomial warp methods in that some points may be corrected more accurately, but others less accurately than a if simple affine transform were used [13]. Thus, greater precision in locating the control points is desired when using higher-order transforms. Six or more control points can

be required to solve for the coefficients of the curvilinear transform. Solving this system of equations requires a general matrix inversion, which can be computationally expensive. Curvilinear transforms do not lend themselves well to piecewise correction and are uncommon in this regard.

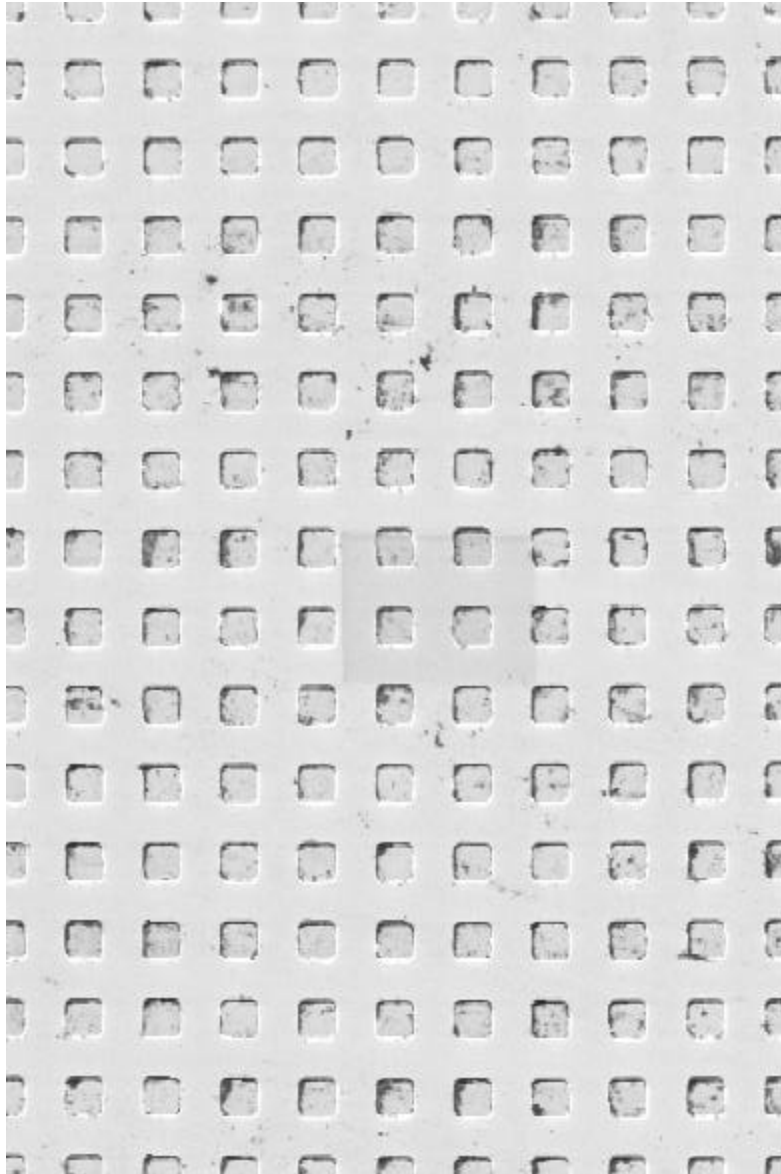
Two issues of precision arise when using the piecewise affine transform: interpolation of data resulting from mapping corrected pixels to non-integer pixel locations in the distorted reference image and interpolation of data corresponding to points lying on the line shared by two triangles in the corrected image. In the case where a pixel in the corrected image maps to a non-integer pixel value in the distorted image, interpolation of data can be performed using bilinear interpolation, zero-order interpolation, or more complex cubic convolution interpolation[7]. Bilinear interpolation is most commonly used because it averages a neighborhood of data, giving a smooth appearance to the final image. The problem with this approach is that sharp transitions are blurred and high frequency content is lost. This loss of information presents problems when the corrected images need to be registered or when the images will undergo image further processing off-line (e.g. edge detection). Using zero-order (nearest neighbor) interpolation gives an image that is not as smooth in appearance, but preserves frequency content and transitions when compared to bilinear interpolation. Zero-order interpolation also has the benefit of being computationally efficient, which cubic convolution ( $\sin x/x$  lowpass filter) is not. Thus, we use zero-order interpolation to avoid the blurring effects and complexity of bilinear interpolation or cubic convolution interpolation. We found better registration of adjacent MIMS sector images using zero-order interpolation. To address the problem of a point lying along a line shared by two triangles, the mapping for both triangles is computed for the one point. The two pixel intensities assigned by the two mappings for this point (from the two different triangle regions) are averaged and assigned to the pixel in the corrected image.

Figure 9 shows the result of correcting the distorted image in Figure 4 with the piecewise affine transform and nearest neighbor interpolation. The correction was performed using twelve evenly spaced control points, as marked in Figure 8. After our correction algorithm, the grid has been correctly restored to rectilinear form. Note that the dimensions of the image have been altered (a result of correcting the demagnification) and that image area outside of regions bounded by control points is removed (because correction is only applied to pixels interior to regions bounded by control points). Compared to the result of SRT correction in Figure 5, our result shows no skewing and all geometric features appear consistently across the image. Measured error in the corrected image shows a maximum of one pixel error. Unlike the SRT corrected image, the error in the piecewise affine transform corrected result is not propagated across the image, so measurable geometric distortion is negligible. A detailed review of the geometric correction algorithm implementation is contained in the following section.



- Figure 8: Reference distorted image with twelve control points marked



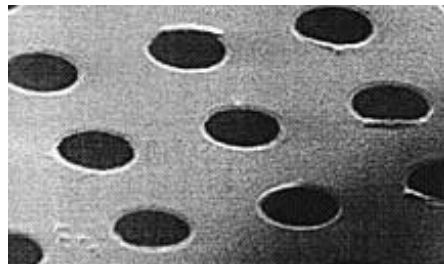


- Figure 9: Piecewise affine transform correction result

## The Correction Algorithm

In this section we will cover the steps for correcting a single SEM image. Implementing the geometric correction begins by taking a reference image of the calibration standard. The image is taken with the SEM configured as it will be used for subsequent images. For this discussion, we will use a reference image of the calibration standard in Figure 10. This standard is made of circular holes of consistent 4 micron center-to-center spacing, but tilt

distortion has occurred. Notice that the circular holes now appear elliptical and the grid arrangement of the holes is not orthogonal. We will now correct the distortion using our algorithm. The landmarks used as control points are the centers of the nine circles (3x3 arrangement). The coordinates of these landmarks are stored in order starting with the top leftmost control point and moving left to right, top to bottom. Note that we could determine the locations of the circles with sub-pixel accuracy through an automated image processing routine, but low-accuracy hand selected locations (one pixel accuracy) are tolerable for SEM images with use of the piecewise affine transform. To demonstrate this, the following example uses coarsely determined landmark coordinates (approximately one pixel accuracy).



• Figure 10: Reference distorted image showing sample tilt distortions

The user enters the ideal pixel spacing between landmarks that would occur in an undistorted image. This number is generally arbitrary (it scales the output image size) but, for consistency and reduced interpolation in real applications, the distance should be determined from the landmark distance occurring at the center (or least distorted region) of the reference distorted image. We choose 60 pixels to equal the distance between the centers of two circles. Since the landmark spacing in the real world (4 microns) distance is known, the pixel to real world conversion is thus defined as 15 pixels equals 1 micron.

An empty buffer, which will contain the corrected image, is generated based on the number of control points and the ideal distance between points. The number of control points  $V$  used in

the reference image along the vertical  $v$ -axis determines the corrected image height and the number of control points  $U$  used along the horizontal  $u$ -axis are used to determine the corrected image width as:

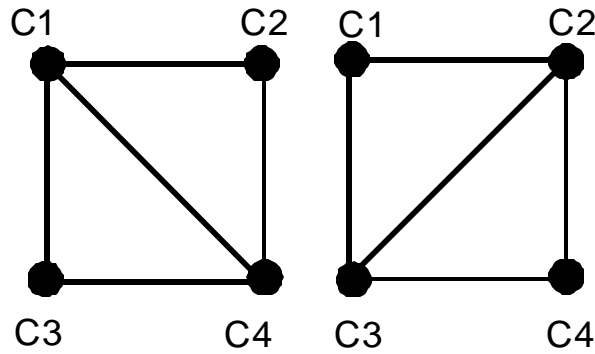
$$\begin{aligned} height &= V + (V - 1) \times dist \\ width &= U + (U - 1) \times dist \end{aligned}$$

where  $dist$  is the user-specified distance in pixels between control points (60 for our example). In this case, we set  $U$  and  $V$  to equal three because of the 3x3 arrangement of circular holes in the image.

The number of triangle primitives  $T$  that can be formed given the number of control points is:

$$T = (V - 1) \times (U - 1) \times 2$$

The eight triangles are organized as in Figure 7a so that the pattern of triangulation over four points alternates between the two possible forms shown in Figure 11. The triangulations in the left of Figure 11 are the triangles with vertices at  $\{C_1, C_3, C_4\}$  and  $\{C_1, C_2, C_4\}$ . The triangulations in the right of Figure 11 are the triangles with vertices at  $\{C_2, C_1, C_3\}$  and  $\{C_2, C_4, C_3\}$ . In general, given the  $k$ -th control point  $C_k$ , a triangulation as shown in the left of Figure 11 is formed as the triangles with vertices  $\{C_k, C_{k+U}, C_{k+U+1}\}$  and  $\{C_k, C_{k+1}, C_{k+U+1}\}$ . The triangulation shown in the right of Figure 11 is formed as the triangles with vertices  $\{C_{k+1}, C_k, C_{k+U}\}$  and  $\{C_{k+1}, C_{k+1+U}, C_{k+U}\}$ . This simple formulation of the triangle vertices works because of the defined ordering of the control points with  $C_1$  being the top left-most control point and with  $k$  increasing from left to right, top to bottom.



- Figure 11: Two possible triangulations over four control points

Some amount of organization is required to ensure that the same triangle is formed over the same control points in the reference distorted image and in the corrected image. This is of course important for assuring that the correct transform is applied to the correct region of the image. Figure 7a shows the alternating pattern of triangulations created for our example. The nine white pixels in Figure 12 indicate where in the corrected image the control points will be placed.



- Figure 12: Ideal locations of the landmarks in the corrected image

The ideal locations of the control points in the corrected image are generated and stored in a list in the same ordering use to store the reference distorted image control points. Regions in the reference distorted image outside of these control points will not be corrected and are discarded by the correction process, thus the corrected image will typically not contain the

information in the borders of the reference distorted image. The top leftmost control point in the corrected image is placed at  $(x,y) = (0,0)$ .

With the local regions defined by eight triangles in both the reference distorted image and the corrected image, the affine correction coefficients for each local region can now be determined. For one triangle region, the reference distorted image control point pixel locations  $(u_i, v_i)$  and the ideal control point pixel locations  $(x_i, y_i)$  are related by the affine transform:

$$u_i = a + by_i + cx_i \quad i=1,2,3$$

$$v_i = d + ey_i + fx_i \quad i=1,2,3$$

This set of three equations and three unknowns for each triangle is written in matrix form as:

$$\begin{bmatrix} 1 & y_1 & x_1 \\ 1 & y_2 & x_2 \\ 1 & y_3 & x_3 \end{bmatrix} \begin{bmatrix} a \\ b \\ c \end{bmatrix} = \begin{bmatrix} u_1 \\ u_2 \\ u_3 \end{bmatrix}$$

$$\begin{bmatrix} 1 & y_1 & x_1 \\ 1 & y_2 & x_2 \\ 1 & y_3 & x_3 \end{bmatrix} \begin{bmatrix} d \\ e \\ f \end{bmatrix} = \begin{bmatrix} v_1 \\ v_2 \\ v_3 \end{bmatrix}$$

To solve for the correction coefficients  $\{a,b,c\}$  and  $\{d,e,f\}$  we only need take a 3x3 matrix inverse, which does not require any specialized algorithm for general matrix inversion.

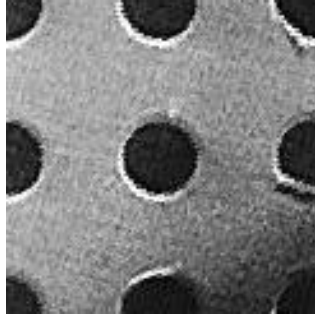
The next task is to determine in which of the eight triangulations a pixel in the corrected image belongs, and hence which correction coefficients should be applied to it. A pixel in the corrected image may lie on the line separating two adjacent triangulations. In this event, the mapping for both triangular regions is computed and the average of both results are used for the intensity value for that pixel.

In order for the correction to work efficiently, a simple algorithm for determining which pixels belong to which local triangle regions is used [10]. A pixel can automatically be determined as being interior to a triangle, exterior to a triangle, or lying on a vertex of a triangle (a point shared by two triangulations). Let  $T(\mathbf{t}_1, \mathbf{t}_2, \mathbf{t}_3)$  be a triangle in two dimensions with  $\mathbf{t}_1, \mathbf{t}_2$ , and  $\mathbf{t}_3$  being 2D row vectors containing the coordinates of the triangle vertices. Given a point  $\mathbf{p}$  (a 2D row vector), we can represent  $\mathbf{p}$  by the parametric equation:

$$\mathbf{p} = \mathbf{t}_1 + q_1(\mathbf{t}_2 - \mathbf{t}_1) + q_2(\mathbf{t}_3 - \mathbf{t}_1)$$

where  $q_1$  and  $q_2$  are scalars. Solving for  $q_1$  and  $q_2$  determines where the point is located relative to the triangle  $T$ . The point  $\mathbf{p}$  is interior to  $T$  or lies on the edge of  $T$  if  $q_2 \leq q_1$ ,  $0 \leq q_1 \leq 1$ , and  $0 \leq q_2 \leq 1$ . Furthermore, if  $q_1 = 1$  and  $0 \leq q_2 < 1$ ,  $\mathbf{p}$  is on the line segment  $(\mathbf{t}_2, \mathbf{t}_3)$ . If  $q_2 = 0$  and  $0 < q_1 \leq 1$ ,  $\mathbf{p}$  is on the line segment  $(\mathbf{t}_1, \mathbf{t}_2)$ . If  $0 < q_1 < 1$  and  $0 < q_2 < 1$  and  $q_1 = q_2$ ,  $\mathbf{p}$  is on the line segment  $(\mathbf{t}_1, \mathbf{t}_3)$ . For all other cases, the point is outside of the triangle  $T$ .

Now that the correction coefficients for every region and the pixels contained in every region are known, any pixel  $(x, y)$  in the corrected image can be mapped to a pixel  $(u, v)$  in the original distorted image. A lookup table is generated giving the mapping of every pixel in the corrected image to its corresponding pixel (or pixels in the case where the corrected point lies on the boundary of two regions) in the distorted image. This lookup table is used for quickly correcting all images taken with the SEM. In the event that the  $(u, v)$  coordinates are non-integers, the nearest neighbor pixel in the distorted image is used by rounding to the nearest integer.



• Figure 13: Corrected image

Figure 13 shows the corrected image resulting from the piecewise affine transform algorithm. Angles formed by drawing lines through the centers of the holes will now be orthogonal and the holes now appear circular. Note that the damage to the holes on the right side of the image is physical, not a result of any distortion. Measurable error is within 1.5 pixels in the final image (with one pixel maximum error due to selection of control points and a half pixel due to nearest neighbor interpolation). Note that because of the nature of the piecewise approach, the error does not accumulate across the image, so geometry is generally unaffected. Automation of the control point selection could improve the error to subpixel levels. Future work will include varying the accuracy of control point locations and varying the number of control points to see how these factors can influence accuracy of the correction.

## Bibliography

- [1] S. Murray and A. Windle, "Characterisation and Correction of Distortions in SEM Micrographs," *Conference on Scanning Electron Microscopy: Systems and Applications*, pp. 88-93, Inst. Physics, UK July 1973.
- [2] *A Guide to Scanning Microscope Observation*, 2<sup>nd</sup> ed., published by JEOL LTD. available at <http://www.jeol.com>
- [3] R. Barrett and C. Quate, "Optical scan-correction system applied to atomic force microscopy," *Review of Scientific Instruments*, vol. 12 no. 6, pp. 1393-1399, June 1991.
- [4] H. Haneishi, Y. Yagihashi, and Y. Miyake, "A new method for distortion correction of electronic endoscope images," *IEEE Transactions on Medical Imaging*, vol. 14 no. 3, pp. 548-555, September 1995.
- [5] R. Marschallinger and D. Topa, "Assessment and correction of geometric distortions in low-magnification scanning electron microscopy images," *Scanning*, vol 19, pp. 36-41, 1997.
- [6] Y. Christophe, J. Cornelius, and P. DeMuynck, "Subpixel geometric correction of digital images," *Signal Processing IV: Theories and Applications*, pp. 1605-1607, 1988.
- [7] R. Gonzalez and R. Woods, *Digital Image Processing*, Addison-Wesley, pp. 296-302, 1993.
- [8] D. Reimann and M. Flynn, "Automated distortion correction of x-ray image intensifier images," *IEEE Nuclear Science Symposium and Medical Imaging Conference Record*, pp. 1339-1341, Orlando, FL, October 1992.
- [9] P. Heckbert, *Fundamentals of Texture Mapping and Image Warping*, Master's Thesis, UCB/CSD 89/516, CS Division, U.C. Berkeley, 1989.
- [10] J. Otto, A. Smith, *Ray-Tracing with Affine Transforms*, MathVision Inc. Technical Journal available at <http://www.olympus.net/biz/7seas/tjour.html>, July 1995.
- [11] J. Lind, L. Ostergaard, O. Larsen, H. Nielsen, N. Bartholdy, and J. Haase, *System for 3D Localisation of Malformations in the Human Brain*, Technical Report, No. 98-3, ISSN 1397-9507, Virtual Centre for Health Informatics, Aalborg University, September, 1998.
- [12] B. L. Adams, et al., "Extraction of Grain Boundary Energies from Triple Junction Geometry", *Proc. of the Twelfth International Conference on Textures of Materials*, Montréal, Canada, NRC Research Press, pp. 9-20, August 1999.



- [13] M. Goodchild, M., *Spatial Statistics and Models*, G. Gaile and C. Willmott, eds., Reidel Publishing Co., Dordrecht, Holland, pp. 33-53, 1984.